Chemical Engineering Journal 493 (2024) 152620

Contents lists available at ScienceDirect

Chemical Engineering Journal

journal homepage: www.elsevier.com/locate/cej

sp^2-rich dendrite-like carbon nanowalls as effective electrode for environmental monitoring of explosive nitroaromatic

Anna Dettlaff [a,b,*], Małgorzata Szopińska [c], Daniel Houghton [d], Piotr Prasuła [e], Yisong Han [f], Marc Walker [f], Geoff West [g], Agata Kamieńska-Duda [e], Sylwia Fudala-Książek [c], Michał Sobaszek [b]

[a] Gdańsk University of Technology, Faculty of Chemistry, 11/12 Narutowicza Str., 80-233 Gdańsk, Poland
[b] Gdańsk University of Technology, Faculty of Electronics, Telecommunications and Informatics, Narutowicza 11/12, 80-233 Gdańsk, Poland
[c] Gdańsk University of Technology, Faculty of Civil and Environmental Engineering, Narutowicza 11/12, 80-233 Gdańsk, Poland
[d] University of Warwick, Department of Chemistry, Coventry CV4 7AL, UK
[e] Military Institute of Armament Technology, Wyszyńskiego 7, 05-220 Zielonka, Poland
[f] University of Warwick, Department of Physics, Coventry CV4 7AL, UK
[g] University of Warwick, WMG, Coventry CV4 7AL, UK

ARTICLE INFO

Keywords:
Trace explosives determination
Electrochemical sensor
2,4,6-trinitrophenylmethylnitramine
Polluted water
Carbon nanowalls
Nitroaromatic compounds

ABSTRACT

Nitroaromatic compounds are commonly used explosive materials that pose a risk to human health and ecosystems due to their acute toxicity and carcinogenicity. Nitroaromatics have numerous pathways into the environment *via* discarded munitions (e.g. into the Baltic Sea after World War II), after use in mining operations, and in industrial run-off from factories producing these compounds (which are produced across the world to date). The current detection method relies on chromatography and mass spectrometry methods, which are time-consuming, expensive, and require specialist equipment and training. Carbon-based electrochemical sensors offer a low-cost, fast, and easy on-site method for the detection of a variety of compounds. This study demonstrates an efficient approach for rapid electrochemical sensing of Tetryl (N-methyl-N-2,4,6-tetranitroaniline) through the use of boron-doped sp^2-rich carbon structures. These structures, known as dendrite-like carbon nanowalls (D:CNW), were fabricated in one-step deposition and extensively characterized to understand the structure and surface chemistry. Electrodes were used to detect a range of nitroaromatic compounds, most notably tetryl in both laboratory and real environmental samples, with an excellent sensitivity of 153.0 μA cm^{-2} ppm^{-1} and a detection limit of 17 ppb. The analytical and electrochemical capabilities of D:CNW electrodes indicate their suitability for extensive environmental monitoring.

1. Introduction

Given their price and simplicity of production, nitroaromatic explosives are an international concern due to their widespread use in both armed conflicts and industries such as mining. Tetryl (TET), which is N-methyl-N-2,4,6-tetranitroaniline, is a common nitroaromatic compound which has found widespread use in the production of warfare agents, especially during World Wars I and II [1]. TET is a highly explosive and time-stable compound, and it is used in military propellants and detonators.

However, TET released into the environment is a significant hazard. TET is easily absorbed into the bloodstream either through skin contact, inhalation or drinking water causing harmful health effects like dermatitis, anaemia, insomnia and respiratory irritation [2,3]. Although available toxicity studies indicate its mutagenic effect on bacteria [4], acute toxicity in mammals [3,5,6], and it is highly toxic to aquatic life [7,8]. TET has not been fully investigated for potential carcinogenic effects [9]. However, based on structure–activity relationship studies, its immunotoxicity potential is likely higher than that of 2,4,6-trinitrotoluene (TNT) [9], which is classed as class C carcinogen [10]. Thus, TET's presence in the environment merits concern [3], and monitoring TET concentrations is significant for human health concerns.

To date, TET can enter the environment in numerous ways e.g. during the disposal of munitions [11] and in wastewater streams from

* Corresponding author at: Gdańsk University of Technology, Faculty of Chemistry, 11/12 Narutowicza Str., 80-233 Gdańsk, Poland.
E-mail address: anna.dettlaff@pg.edu.pl (A. Dettlaff).

https://doi.org/10.1016/j.cej.2024.152620
Received 5 March 2024; Received in revised form 6 May 2024; Accepted 27 May 2024
Available online 27 May 2024

their production [12]. In addition, TET is still present in land mines [11], and has been found in many hazardous waste sites [13], where its concentrations in the soil can reach as high as 84,400 mg/kg [14]. In the past, hazardous chemicals, including TET, have been improperly disposed of in clean water bodies, such as lagoons, seas, rivers, and lakes [14]. For example, a discharge of wastewater containing 400–460 mg/L of TET into drainage ditches was documented [14], causing a significant release of tetryl into the environment. Presently, it is important to continuously monitor TET factories to avoid the release of these compounds into the environment.

The most commonly used technique for detecting TET presence in aquatic solution is chromatography coupled with mass spectrometry [15–17]. Despite the high sensitivity, measurement of samples using this technique is relatively expensive, as well as requiring cumbersome sample preparation, and due to the delicacy of the apparatus, it is unreasonable to measure samples in the field. A promising approach involves the utilization of electrochemical sensors (ECs) that record the distinctive electrical signal specific to the analyte. ECs can be used for both qualitative and quantitative analysis, characterised by fast response times, high accuracy, and are cost-effective [18].

Among the different materials utilised as electrode material for electrochemical sensors, the physical and electrochemical properties of carbon make it one of the most commonly used materials in electrochemical sensors [19,20]. The variety of carbon morphologies makes it suitable for a wide range of pollutant sensing applications including drugs, pesticides, heavy metals, *etc*. [21–23].

Nitroaromatic compounds can be detected with great sensitivity on carbon electrodes that have a high content of sp^2-hybridized carbon [24]. This is because, nitroaromatics have in their structure an aromatic ring containing delocalized π electrons, which can interact with the sp^2 surface of the electrode due to π-π electron donor–acceptor stacking interactions [25,26]. Based on this mechanism, nitroaromatic explosive compounds have been detected on glassy carbon [27], graphene [28], carbon nanotubes [29], and boron-doped diamond/graphene nanowall electrode [25,30]. None of these publications concentrate on detecting of TET specifically.

In this work, we use sp^2-rich dendrite-like carbon nanowalls (D:CNW) synthesized using one step chemical deposition process, as a novel approach for rapid electrochemical sensing of TET. The D:CNW layer is successfully doped with boron, which is a key factor to improve the electrical and electrochemical behaviour of carbon nanostructures. The distinctive dendrite-like architecture of the carbon electrode offers an increased surface area facilitating enhanced analyte adsorption, which results in high sensitivity of nitroaromatic compounds detection. In addition to an in-depth analysis of the detection capabilities of D:CNW against TET, the electrode was also tested for the detection ability of other nitroaromatic compounds, such as TNT, 2,4-dinitrotoluene (2,4-DNT), and 2,6-dinitrotoluene (2,6-DNT). Our investigation reveals that the sp^2-rich dendrite-like structure of D:CNW, coupled with its high conductivity and long stability in aquatic solutions, make it a highly promising electrode material for achieving fast and cost-effective electrochemical detection of explosive materials, especially in environmental and industrial monitoring.

2. Experimental

2.1. Chemicals

Hexaammineruthenium (III) chloride (RuHex) $[Ru(NH_3)_6]Cl_3$ (98% purity), 2,4-DNT (97% purity), 2,6-DNT (98% purity) were purchased from Sigma Aldrich, Germany. KCl (99.5% purity), Na_2SO_4 (≥99% purity), Na_2HPO_4 (≥99% purity), KH_2PO_4 (≥98% purity) were acquired from Chempur, Poland. All chemicals were of analytical grade and utilized without additional purification.

The TNT and TET explosives were obtained from a 120 mm mortar projectile and standard booster, respectively and purified for testing purposes by the Military Institute of Armament Technology (Zielonka, Poland). The purification process consisted of 3 recrystallizations from acetone and a constant weight drying procedure. Selected properties of the explosives used in the tests are presented in the Table S1, SI 1.

2.2. Preparation of solutions

Because nitroaromatic compounds exhibit limited solubility in water, TET standard stock solutions of 10, 100, 1,000, 10,000 ppm were made in acetonitrile of HPLC-grade purity (Sigma Aldrich, Germany). 3 other nitroaromatic compounds: TNT, 2,4-DNT, 2,6-DNT of 1,000 ppm each were also made dissolved in acetonitrile.

Aqueous solutions of nitroaromatic compound were made by spiking an aliquot volume of stock solution into 0.1 M phosphate buffer solution (PBS) at pH of 6.75. In this way, the following TET concentrations of 3.9 ppb, 7.8 ppb, 15.6 ppb, 31.3 ppb, 62.5 ppb, 125 ppb, 0,25 ppm, 0.5 ppm, 1 ppm, 2 ppm, 4 ppm, 8 ppm, 16 ppm, 32 ppm were obtained. Additionally, 1 ppm solutions in 0.1 M PBS at 5.70 pH of TET, TNT, 2,4-DNT, 2,6-DNT were created.

TET was also detected in a more complex background electrolyte, from environmental samples described in section 2.5. These samples were prepared similarly to the PBS standard samples – aliquots of the TET stock solutions were added to environmental samples resulting in concentrations 3.9 ppb – 32 ppm. Due to the low conductivity of the environmental solutions, Na_2SO_4 background electrolyte was added to them to a final concentration of 0.05 M.

Tests based on the pH of the solution have been performed by varying the pH of the 0.1 M PBS buffer, made to pH = 5.70 (± 0.02), 6.75 (± 0.01), and 8.00 (± 0.01) were made by mixing corresponding volumes of 0.2 M Na_2HPO_4, 0.2 M KH_2PO_4, and deionised water (DI) with ionic conductivity of 0.05 μS/cm.

An additional test was conducted to detect 2 ppm 2,4-DNT using three different electrodes: a glassy carbon (GC) disc electrode (ϕ = 3 mm, Mineral, Poland), boron-doped diamond that was grown according to [31] without any post-treatment method ($BDD_{as\ grown}$), and boron-doped diamond that underwent post-growth chemical treatment ($BDD_{acid\ cleaned}$) to remove sp^2 phase impurities using hot aqua regia, hot 'pyranha' solution, and hydrogen plasma treatment resulting in H-terminated diamond (according to the cleaning procedure in [31]).

2.3. Electrode growth

D:CNW electrodes were prepared by growing on *p*-type ⟨1 0 0⟩ -oriented silicon wafers (7 mm × 7 mm dimensions, 500 ± 25 μm thickness, 1 – 10 Ω cm resistivity – see Fig. S1a, SI 2) using a microwave plasma-enhanced chemical vapour deposition system – MPECVD (SEKI Technotron, model AX5400S, Japan). Before conducting D:CNW growth, the silicon substrates underwent seeding through sonication in a water based nanodiamond slurry for 20 min. The deposition was performed at a plasma power of 1300 W and microwave radiation of 2.45 GHz, at the pressure of 50 Torr, and substrate temperature of *ca.* 800°C for 5 h. The boron-to-carbon ratio of gas mixtures (diborane (B_2H_6) – boron precursor, and CH_4 – carbon precursor) was set to 6,000 ppm. The molar ratio of CH_4/H_2 in gas mixture was kept at 12 % at 165 sccm total flow rate. A nitrogen admixture (3 sccm) was added as catalyst of D:CNW growth.

2.4. Characterisation techniques

A Zeiss Gemini FE-SEM 500 field emission scanning electron microscope (FE-SEM) was used to image the surface of D:CNW utilizing the in-lens detector at 5 kV.

Scanning transmission electron microscopy (STEM) observations were conducted in a JEOL ARM200F TEM, operated at 200 kV. An electron transparent sample of D:CNW was prepared by using a standard focused ion beam (FIB) lift-out procedure [32]. Prior to the FIB sample

preparation, a protective titanium layer of approximately 200 nm thick was sputter deposited (NanoPVD-S10A, Moorfield, United Kingdom) to prevent the damage to the underlying D:CNW during the FIB milling process. Briefly, two trenches are cut using a gallium ion beam, then the sample is lifted out as a lamella and attached to a support grid, where it is then further thinned to electron transparency. Annual dark field (ADF) STEM images were then taken from the FIB lamella. Electron energy loss spectroscopy (EELS) spectra were acquired in STEM mode at an energy resolution of 0.9 eV, measured from the full width half maximum (FWHM) of the zero-loss peak with a spectrometer semi-collection angle of 25 mrad; probe convergence semi-angle of 30 mrad and a dispersion of 0.1 eV per channel.

Confocal InVia, a micro-Raman spectrometer from Renishaw, was used to collect Raman spectra of D:CNW electrodes. An excitation wavelength of 514 nm, generated by an Ar ion laser, was employed. The wavenumber range covered 100 to 3200 cm^{-1}.

A Kratos Analytical Axis Ultra DLD spectrometer with a monochromatic Al Kα X-ray source (1486.69 eV) was used for X-ray photoelectron spectroscopy (XPS). The pressure of XPS chamber was below 1 $\times 10^{-10}$ mbar. The measurements were conducted at room temperature and at a take-off angle of 90° with respect to the surface parallel. The core level spectra were recorded using a pass energy of 20 eV (resolution approx. 0.4 eV), from an analysis area of 300 × 700 mm. The work function and binding energy scale of the spectrometer were calibrated using the Fermi edge and $3d_{5/2}$ peak recorded from a polycrystalline Ag sample prior to the commencement of the experiments. For compositional analysis, the analyser transmission function has been determined using clean metallic foils to determine the detection efficiency across the full binding energy range. To investigate the chemical composition of the D:CNW electrode surface, all data collected were fitted in CasaXPS. A Shirley-type background was subtracted from C 1s, O 1s, B 1s spectra, whereas linear background correction was performed for N 1s spectrum. Signals were fitted with mixed symmetric Gaussian-Lorentzian lineshape or with asymmetric lineshape (signals: 284.1 eV of C 1s; 397.2 eV and 398.2 eV of N 1s; 186.0 eV, 187.4 eV, 188.6 eV of B 1s). Before XPS measurements, samples were heated up in the tube furnace (Lindberg/Blue M™, Thermo Fisher Scientific, Ltd.) to 500°C for 1 h under argon, to reduce adventitious carbon contamination at the surface.

The electrical conductivity of D:CNW electrode was measured using four-point probe (Pro4, Signatone, USA) connected with source measure unit (Keithley 2450, Tektronix, UK).

The electrochemical investigations were carried out employing a potentiostat–galvanostat instrument (VMP-300, Bio-Logic, France) controlled by the EC-Lab software. Electrochemical tests were performed within a three-electrode cell (WE: D:CNW; CE: platinum coil; RE: Ag/AgCl/3M KCl or Ag/AgCl wire – see Fig. S1b, SI 2) at room temperature (22 ± 1 °C). The electrochemical measurement was performed in a 2 mL solution each time. All solutions were deoxygenated before measurements. The geometric surface of the working electrode was determined by a 4 mm diameter silicone gasket. DI water having an ionic conductivity of 0.05 μS/cm was utilised to create the solutions for electrochemical analyses.

Electrochemical characterization measurements of D:CNW electrodes were conducted using cyclic voltammetry (CV) and electrochemical impedance spectroscopy (EIS) in 1 mM $[Ru(NH_3)_6]Cl_3$ solution in 1 M KCl. Additional CV experiments were performed in 0.1 M PBS at ν = 100 mV s^{-1}, in order to determine a solvent window for D:CNW electrodes. CV *vs* scan rate was also recorded at the 5, 10, 25, 50, 100, 200, and 300 mV s^{-1} to examine electrode kinetics. Electrochemical behaviour and stability tests were carried out using EIS. EIS were measured with an amplitude of 10 mV in the frequency range from 25 mHz to 100,000 Hz (10 points per frequency decade). Electrochemical impedance spectra tests were performed at the formal potential (E_f) (the working electrode was stabilized at E_f for 10 min), which was calculated from Eq. (1) based on single CV cycle:

$$E_f = \frac{E_{pa} + E_{pc}}{2} \quad (1)$$

where E_{pa} and E_{pc} corresponds to the potential of anodic and cathodic peak, respectively.

DPV was used as a nitroaromatic detection technique. The DPV technique was selected due to its extensive use in the detection of nitroaromatic compounds [33–35], as well as our prior research on explosive compound detection employing this method [25,30]. A parameter optimisation experiment (Fig. S2, SI 3) was conducted to optimise the D:CNW response. Based on the highest current obtained, the optimum value for pulse width was determined to be 20 ms (Fig. S2a, SI 3). Measurements were then taken to determine pulse height. Considering the values of the reduction peaks currents (Fig. S2b, SI 3) and on the background height, a value of 110 mV was chosen. Step height of −5 mV and step time of 500 ms were selected based on peak shape. Differential pulse voltammograms were collected by applying a potential that varied from 0 V to −0.8 V (*vs* Ag/AgCl/3.0 M KCl). Before DPV measurements, samples were conditioned by polarising from 0 to −0.8 V until the background response was stabilised. All current density values were calculated basing on geometric surface area of D:CNW electrode, and thus represent an underestimate for the true current density.

Based on the results of detection currents of TET, the limit of detection (LOD) was calculated using Eq. (2) [25,36,37]:

$$\mathrm{LOD} = \frac{3\sigma_{bl}}{a} \quad (2)$$

where σ_{bl} reflects the standard deviation of a blank, and "a" denotes the slope of the calibration curve.

2.5. Environmental samples

Different environmental samples have been taken as a background matrix for TET detection. Industrial or post-industrial areas in Poland have been selected: (1) the former area of "Zachem Chemical Plant" in Bydgoszcz, where freshwater sample (**ZCP**) were collected and (2) the area of the Municipal Waste Management Plant (MWMP) in Gdańsk Szadółki, where water sample from a piezometer at the tributary of the landfill (**MWMP-P**) and a water sample from the plant's deep well (**MWMP-W**) acting as a reference point were taken. Environmental sampling site descriptions and real-life sample characterisation can be found in SI 4.

3. Results and discussion

3.1. Material characterisation

A thorough investigation utilizing a SEM was undertaken to examine the surface morphology of the D:CNW electrode growth (Fig. 1a; Fig. S3, SI 5). The resulting film exhibits remarkable homogeneity and continuity, as evidenced by Fig. S3a, SI 5. Notably, the average thickness of the carbon layer falls at 3.97 μm ± 0.18 μm, calculated from 15 cross-sectional measurements depicted in Fig. S3b, SI 5.

To further characterise the D:CNW layer, a cross-sectional analysis was performed using a lamella from FIB cutting the sample inside the STEM. The D:CNW sample's cross-section, shown in Fig. 1b, illustrates the growth of the D:CNW carbon structure (the sample was cut all the way down to the silicon substrate). As can be seen, the electrode morphology exhibits extensive development reminiscent of dendritic structures. These complex branched dendrite formations begin to manifest in the early stages of deposition. Using Gwyddon 2.60 software (Czech Republic), the estimated dimensions of the dendrites were measured (derived from a set of 7 measurements). The length of a solitary dendrite core is comparable to the thickness of the D:CNW

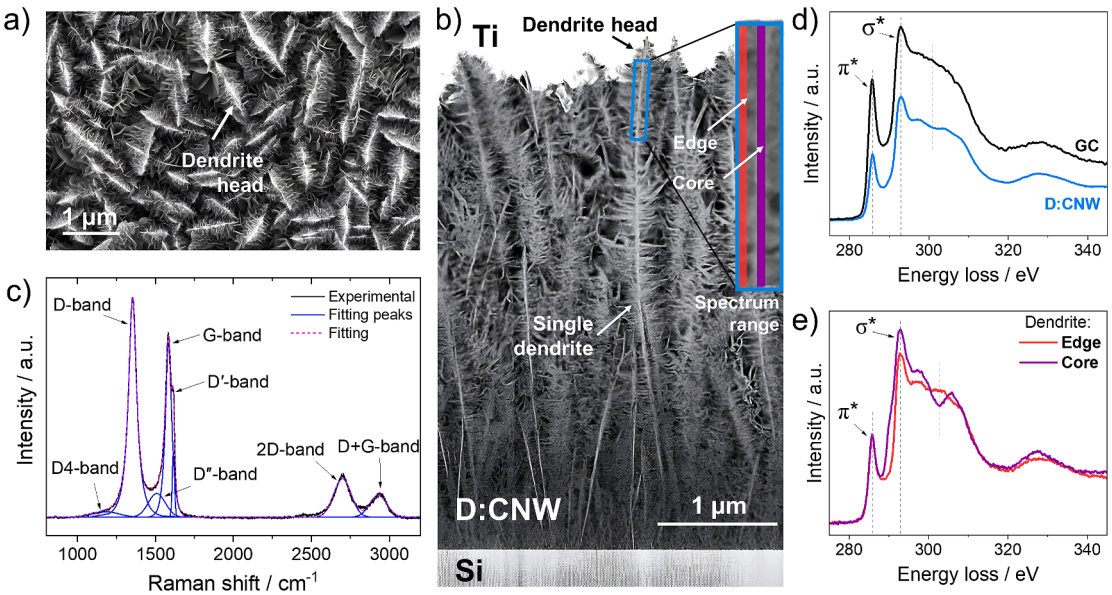

Fig. 1. Morphology and structure characterisation of D:CNW electrode: a) In-lens SEM image of D:CNW surface; b) ADF STEM image of D:CNW FIB cross section; inset: the regions where EELS spectra are taken highlighted; c) fitted Raman spectra of D:CNW; High loss EELS spectra of d) crushed GC (black) compared to D:CNW (blue) taken over the full spectrum area, e) dendrite edge (red) compared to dendrite core (purple), illustrated in Fig. 1b inset.

electrode (4.20 ± 0.05 µm). The length of the dendrite is expected to be influenced by the growth period in a similar manner to how the thickness of the carbon layer depends on the duration of the MPECVD process. The thickness of horizontal branches varies according to their specific position. The branches in the central region of the dendrite are the longest, measuring roughly 182 ± 47 nm. The length of the branches close to the substrate is 86 ± 12 nm, while the breadth near the top is around 112 ± 3 nm. The width subsequently decreases to a single nanometer at the upper border of the dendrite. This intricate surface structure is significantly different from the carbon structure typically found in literature [38–46], which exhibit a nanowall-like form without any branching. To our knowledge, there have been no previous reports of carbon-nanowall structures with this level of complexity. The samples clearly have a highly structured surface, with a high aspect ratio, which we believe originates from the growth conditions, including a high methane content, boron admixtures, and elevated temperature.

Raman spectra of D:CNW surface are shown in Fig. 1c. Two major peaks are identified at 1352 cm^{-1} and 1582 cm^{-1}, which correspond to the D-band and G-band, respectively. The D-band signifies a flaw in the graphitic structure, stemming from out-of-plane vibrations, while the G-band arises from in-plane vibrations of the C-C bond within the sp^2 orbital, indicating the presence of graphitic structure [47]. The intensity ratio between the D- (I_D) and G-bands (I_G) is *ca.* 1.99, which, according to the literature, corresponds to a highly sp^2-rich carbon surface [48–50]. Secondary bands, known as D′ and D″, are attributed to C=C bond and structural disorder or defects, respectively [51]. Notably, the D′ band is characteristic of structures with relatively low levels of disorder, such as graphite-like carbons and glassy carbon, but is not observed in highly disordered carbon forms like carbon black. The peak observed at 1180 cm^{-1} reflects the D4-band, and it is ascribed to the presence of TPA (*trans*-poly acetylene) [52] and is conjugated with increased hydrogen content [53] (film is deposited in rich hydrogen plasma).

Additional bands are also evident, including an intense band originating from the second harmonic of the D-band (2D), which is associated with crystalline graphitic structures [54]. Another observed band, the D+G band, is attributed to a defect-induced double resonance intervalley scattering process [55]. The summary of the fitting spectra is shown in Table 1.

To verify the repeatability of the CVD process, Raman spectroscopy measurements were carried out on 3 independent CVD processes (Fig. S4, SI 6), which shows Raman spectra with the same bands as shown in Table 1, which confirms the repeatability of the D:CNW growth process in terms of chemical composition.

Table 1
Fitting of characteristic Raman bands of D:CNW.

Centre of peak / cm^{-1}	Percent of the total area / %	Classification	Ref.
1180	2.8	D4-band	[55]
1352	42.5	D-band	[51]
1508	7.8	D″-band	[51,56]
1582	23.8	G-band	[51]
1615	2.9	D'-band	[51]
2698	12.9	2D-band	[57]
2928	7.3	D+G-band	[55]

The D:CNW structure was then examined by electron energy loss spectroscopy to estimate the bonding character of which the material is composed. The Fig. 1d shows EELS spectra of the carbon K-edge spectra of D:CNW and glassy carbon (GC) electrode, with the latter serving as a reference material containing 100 % sp^2 bonded carbon [58] in this experiment. As can be seen, both spectra are composed of two major and well-defined peaks. The peak at 293 eV reflects the excitation of the 1s core level electrons to unoccupied anti-bonding σ* states, whereas the second signal is placed at ~ 286 eV and it originates from 1 s → π* transition, labelled in Fig. 1d [59]. The presence of a peak at about 286 eV is related to the presence of an sp^2-rich phase in the carbon structure, and in the case of materials made only of sp^3-hybridised carbon, this peak does not appear at all [59,60]. It can be observed that the π* peak is significantly higher for a GC electrode suggesting that D:CNW material is not purely sp^2 material. Thus, the sp^2: sp^3 bonding distribution in the layer was calculated using the two-window method proposed by Bruley *et al.* [61]. To achieve this, the spectrum obtained for GC, was compared to the D:CNW spectrum in Fig. 1d, taken over the entire spectrum region of D:CNW (blue rectangle in Fig. 1b). This method takes the ratio between the integral intensity over the π* region (280 – 290 eV; window 1), and the integral intensity over π* + σ* (280 – 300 eV) for both glassy carbon and for D:CNW. In glassy carbon the ratio between the two peaks was 0.257, which we assign as 100% sp^2 [58]. The same treatment was applied to the D:CNW data, which was calculated to be 78% of GC

intensity (*i.e.* 78% sp^2).

It was observed that the sp^2 carbon content varies slightly between the centre and edge of the dendrite. At the edge of a single dendrite (red highlighted area of inset Fig. 1b), the content is higher at 78%, while in the dendrite's core (purple highlighted area of inset Fig. 1b) it is only 73%. This difference in sp^2 content amount could be explained by the fact the core nucleates grow from the sp^3 nanodiamond particles [62]. This is supported by the observation that the spectrum obtained for the core which differs from that taken at the edge of the dendrite showing the presence of characteristic for sp^3 carbon gap visible at *ca.* 303 eV [63].The discernible variation in the carbon structure is also noticeable for the shape of the spectra seen in Fig. 1e.

The elemental composition and the chemical bonds on D:CNW surface were examined *via* X-ray photoelectron spectroscopy (Fig. 2). The peak fitting for the C 1s spectrum is shown in Table 2. The XPS survey spectrum, depicted in Fig. 2a, illustrates the presence of carbon, oxygen, nitrogen, and boron. Carbon is the basic building material of the electrode layer, reaching an atomic concentration of 96.6 at%. Based on the XPS C 1s spectrum (Fig. 2b), eight carbon components of different origins were discerned. The main asymmetric peak observed at 284.1 eV represents sp^2 C=C carbon and reaches 73.1% of total carbon, whereas the peak at 284.6 eV can be attributed to sp^3 C-C carbon bonds. The D:CNW electrodes have been effectively doped with boron, which is crucial to enhancing the electrical and electrochemical properties of carbon nanowall-like structures [64], as evidenced by the presence of peaks at 282.7 eV on the C 1s spectrum (high resolution B 1 s is presented in (Fig. S5a, SI 7). The total amount of embedded boron is estimated to be 1.7% from the relative integral intensities of the C 1s *vs* the B 1s.

Apart from the incorporated boron, small amounts of nitrogen and oxygen (~0.9% each, based on relative integral intensities C 1s to N 1s / O 1s) are also evident in the layer (Fig. S5b, SI 7). The presence of oxygen is probably due to contamination of the sample with atmosphere oxygen [71]. Nitrogen incorporation into the sample derived from the nitrogen gas used in the MWECVD process, which catalyses the growth of nanowall structures. According to the literature [72], the simultaneous presence of nitrogen, which has one extra electron compared to carbon, and boron, which has one less electron, should result in a charge compensation, which will result in a decrease in the charge carrier concentration. In the case of D:CNW material, the impact of the charge compensation process is expected, however, it should be noted that the amount of boron built into the layer far exceeds the amount of incorporated nitrogen. Moreover, the amount of boron is sufficient to provide adequate conductivity for electrochemical purposes (D:CNW electrode has a high electrical conductivity of 1.14×10^5 S/cm estimated through four-point probe testing, resulting in efficient electron transfer and more effectively facilitates electron transfer at the electrode–electrolyte interface [73]). It should be emphasize, that the incorporation of nitrogen atoms into D:CNW is low, despite the relatively high reactor feed gas ratio of N:C = 0.5, but the XPS indicates less than 1% uptake into the sample. The unique structures have arisen from complex growth mechanism involving multi-species interactions beyond CN^-, H_yCNH_x, BH^-_x and CH^+_x radicals [64,74]. The low nitrogen content can be explained by the growth mechanism where primarily the CN^- radicals are present on the growth surface, serving as attachment points for other carbon radicals. This interaction initiates the process of nitrogen abstraction through the bonding of CH_3 groups, thereby actively participating in the intricate mechanism underlying the formation of nanowalls. Moreover, it plays a pivotal role in facilitating the nucleation of twin formations within the subsequent layer of nanowalls, thereby influencing their structural development and eventual properties [60]. In the context of boron atoms, derived from BH^-_x radicals, are integrated into the D:CNW structure [74]. Following that the nitrogen in indispensable for forming and growing carbon nanowall structures without any external catalyst [74].

Table 2
Contributions of the components in the C 1 s spectra of the D:CNW samples.

	Binding Energy / eV	Relative composition / %	Assignment	Ref
C 1 s	282.7	2.6	C-B	[65]
	284.1	73.1	C = C (sp^2)	[66]
	284.6	6.6	C-C (sp^3)	[66]
	286.2	5.4	C-O / C-N / C-O-C	[66,67]
	287.5	1.5	C = O / N-C = O	[67,68]
	288.5	1.6	O-C = O	[66]
	290.5	7.6	π-π*	[68,69]
	293.5	1.6	π-π*	[70]

Analysis of the XPS spectra also allows for an evaluation of sp^2 to sp^3 carbon ratio by determining the *D*-parameter proposed by Lascovich *et al.* [68,75]. The *D*-parameter was established by measuring the distance between the highest and lowest points visible on the first-order differential of the carbon Auger peak (Fig. 2c), resulting in $D = 20.2$ eV. Due to the linear dependence of the *D*-parameter on the carbon content of the sp^2 hybridisation [68,75], where diamond = 14.2 eV and graphite = 22.5 eV, the D:CNW layer contains approximately 74% sp^2 carbon.

The electrochemical behaviour of D:CNW was comprehensively tested using CV and EIS (Fig. 3). First, the solvent window in 0.1 M PBS was established for a geometric current density of ± 0.35 mA cm^{-2}, which corresponds to the points at which solvent (water) electrolysis becomes distinguishable from the background currents (Fig. 3a). D:CNW electrode exhibits a quite wide solvent window of 2.82 V, which will allow the detection of nitro compounds whose reduction potential is predominantly in the 0 to −1 V range.

Four slight peaks could be visible at −0.41 V, −1.25 V, +0.05 V, and +1.15 V (*vs* Ag/AgCl/3M KCl). The occurrence of these signals might may be attributed to the oxidation and reduction of functional groups located on the electrode's surface in particular oxygen groups such as quinone, carbonyl, and ketone moieties [76,77]. The presence of these groups has previously been confirmed in XPS testing (see Table 2).

The electrochemical kinetics was studied using the outer-sphere electron, one-electron transfer, RuHex redox mediator (Fig. 3b-c). As can be seen in CV in Fig. 3b, the peak-to-peak separation, ΔE_p, representing the potential distance between the peak maximum of $[Ru(NH_3)_6]^{2+}$ oxidation and the peak of $[Ru(NH_3)_6]^{3+}$ reduction ($\Delta E_p = |E_p$

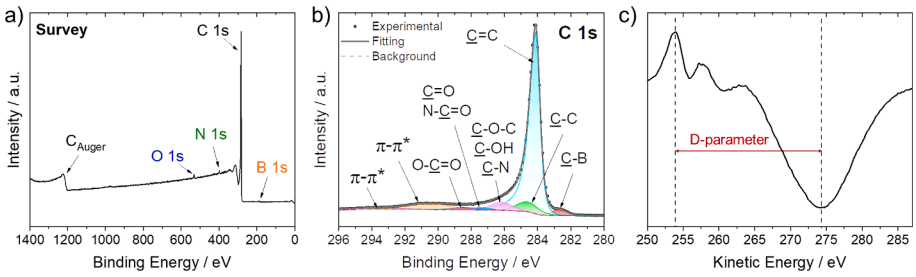

Fig. 2. D:CNW electrode XPS results: a) survey spectrum, b) high resolution spectra of C 1s, c) the first differential of C_{Auger} peak.

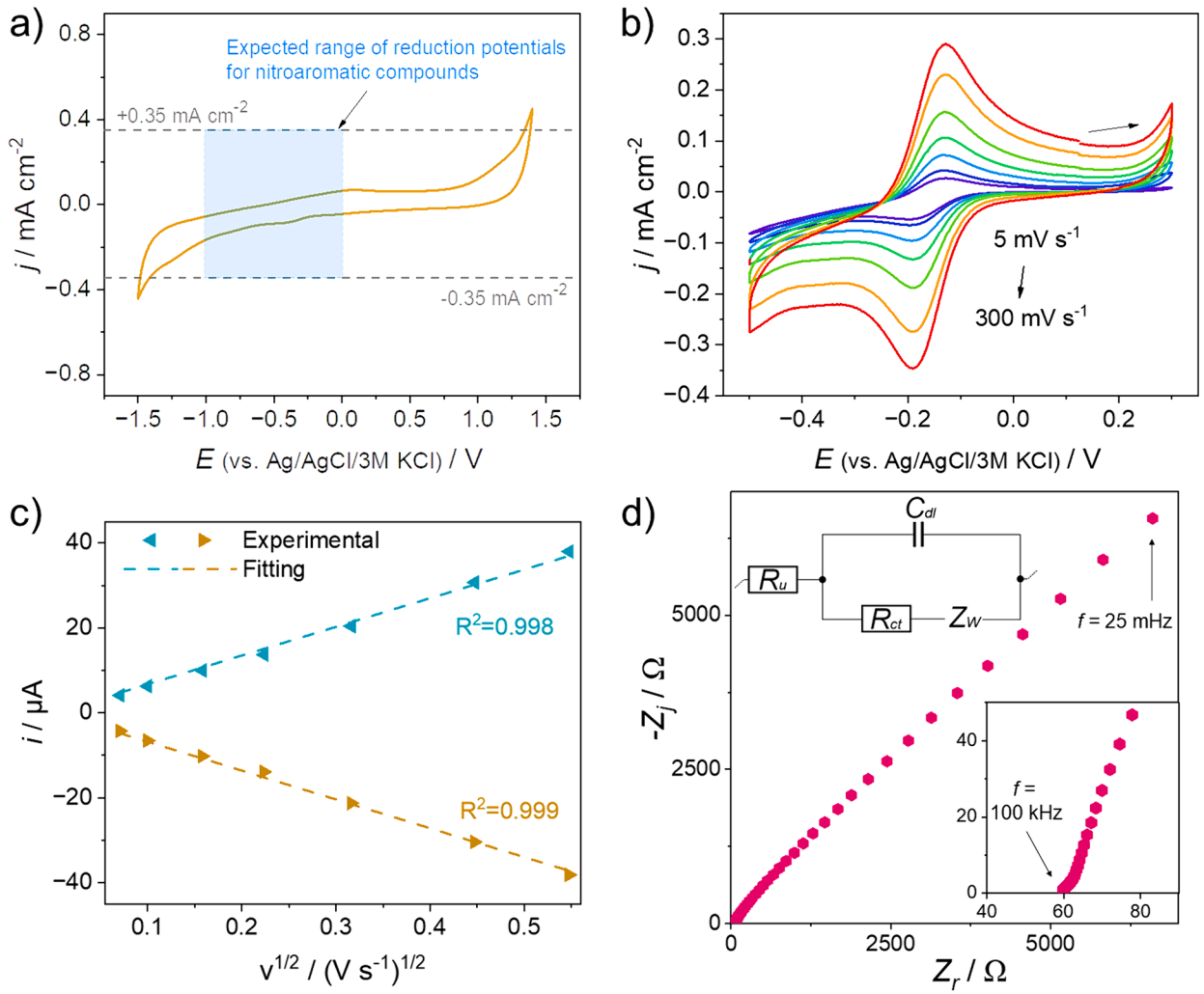

Fig. 3. Electrochemical behaviour of D:CNW recorded in 0.1 M PBS (pH = 6.75) a) cyclic voltammetry recorded at scan rate 100 mV s^{-1}, and 1 mM $[Ru(NH_3)_6]Cl_3$ solution in 1 M KCl: b) cyclic voltammogram recorded as a function of scan rate; c) dependence of the peak current on the square root of scan rate (based on results from Fig. 3 b); d) Nyquist representation of EIS (inset: EEC used for fitting).

$_{ox} - E_{p\ red}$| [78]), is practically independent of scanning rate. For the slowest scan rate (5 mV s^{-1}), the value of ΔE_p is 60.7 mV, whereas for the 300 mV s^{-1} ΔE_p increases to 62.7 mV (see Table S3, SI 8). The obtained values of ΔE_p are very close to the theoretical value of the complete electrochemically reversible process calculated using Eq. (3) [78] (56.4 mV in 22 °C):

$$\Delta E_p = 2.218\frac{R \cdot T}{n \cdot F} \quad (3)$$

R – gas constant [8.314 J K^{-1} mol^{-1}]; T – the temperature [295 K]; n – the number of electrons [–]; F – Faraday's constant [96,485 C mol^{-1}].

The anodic and cathodic peak currents, $i_{p\ ox}$ and $i_{p\ red}$, exhibit a direct proportionality to the square root of the scan rate (Fig. 3c) and the $i_{p\ red}$: $i_{p\ ox}$ is almost 1.0 regardless of the scan rate (see Table S3, SI 8). Both of these phenomena are indicative of reversible redox reactions [79,80], which indicates D:CNW have rapid electron kinetics, highlighting its suitability for electrochemical sensing applications.

EIS measurements were obtained to gain more insights into the electrochemical processes occurring at an electrode–electrolyte interface. In order to extract information about the system's response to varying frequencies of applied AC voltage, the EIS experimental data were fitted using an electrical equivalent circuit (EEC). A Randles circuit [81] (Fig. 3d inset) was chosen as an appropriate EEC. It consists of 4 components: *i)* the uncompensated resistance – R_u (the electrolyte resistance between WE and RE electrodes, the resistance of WE itself, and resistance of connection); *ii)* a capacitor related to the capacitance of the electrical double layer – C_{dl}; *iii)* resistor reflecting the charge transfer resistance – R_{ct} (equal to the diameter of a semicircle at high-frequency region); *iv)* a Warburg impedance element, Z_W, represented by a straight line in low frequency region, in which the potential is maintained for a sufficient duration, leading to species depletion in the electrode's proximity, causing the increase in impedance [81]. Utilizing the fit, an R_u equal to 6.5 ± 0.8 Ω cm^2 (measured using 4 different electrodes), whereas the electrode double layer capacitance is relatively high at 66.8 ± 19.3 µF cm^{-2} (Table S4, SI 8), this value is not only from high intrinsic capacitance but also from the high electrode surface area as is the case with other carbon nanowall structures [45]. The electrode is also characterised by a charge transfer resistance of 0.5 ± 0.2 Ω cm^2. The D:CNW electrode demonstrates a comparatively low value of R_{ct} when compared to other carbon materials with sp^2 content measured in RuHex redox pair: *i)* nanosized graphene sheets R_{ct} = 1.19 – 4.13 Ω cm^2 [82], *ii)* as grown boron-doped diamond (BDD) showed R_{ct} of 9.8 Ω cm^2 [22], *iii)* conductive printable electrodes tuned by boron-doped nanodiamond foil additives R_{ct} = 15.0 Ω cm^2 [37]. The notably low R_{ct} value achieved by D:CNW material suggests rapid charge transfer, which may originate from a high content of boron dopant, uniform electrode coverage and an interconnected network of D:CNW that can improve electron transport pathways.

Based on the R_{ct} value, which manifests the kinetics of heterogeneous charge transfer, heterogeneous electron transfer (HET) rate constant, k° [cm s^{-1}], was determined using Eq. (4) [22,83]:

$$k^{\circ} = \frac{R \cdot T}{n^2 \cdot F^2 \cdot A \cdot C \cdot R_{ct}} \quad (4)$$

where R represents the molar gas constant with a value of 8.314 J mol^{-1} K^{-1}, T stands for the temperature [298 K], n reflects the number of electrons [1], F is the Faraday constant [96,485 C mol^{-1}], A [cm^2] is attributed to the geometric electrode area, and c [mol cm^{-3}] corresponds to the concentration of redox mediator.

k° value estimated for RuHex redox reaction recorded on D:CNW electrode reached 6.67 × 10^{-1} cm s^{-1} (± 2.16 × 10^{-1} cm s^{-1}). The value is in close proximity to the HET value associated with a completely reversible electrochemical process, which is typically expected to be equal to or greater than 1 cm s^{-1} [84]. Obtained for D:CNW electrode k° value is also higher than the HET values found in the literature for 'classical' nanowall electrodes [83,85].

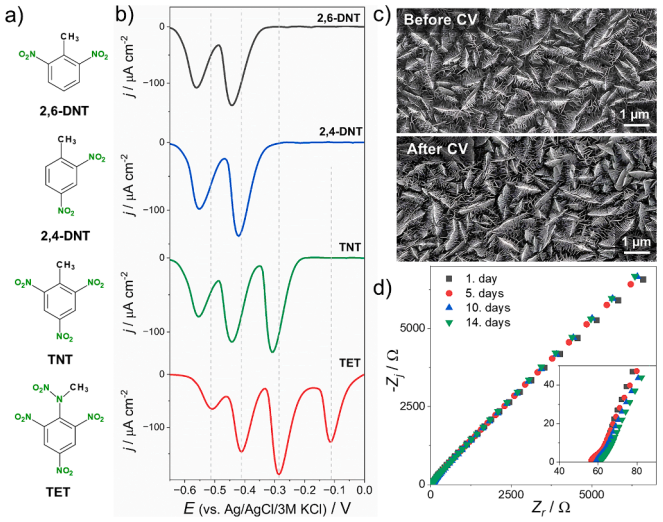

Fig. 5. a) Chemical structures of examined nitroaromatic compounds (2,6-DNT, 2,4-DNT, TNT, TET); b) current responses of compounds shown in Fig. 5a recorded on D:CNW in 0.1 M PBS, pH = 5.70 (data after background subtraction); c) SEM × 10,000 magnification before and after 3,000 cycles; d) Nyquist plot of impedance spectra of selected D:CNW electrode recorded 1 mM RuHex in 1 M KCl at the formal potential over a period of 14 days.

3.2. Electrochemical detection of tetryl

First, TET detection using the DPV technique was performed in a laboratory-grade, 0.1 M PBS solution at a pH close to neutral (pH = 6.75) with a known concentration of the explosive material. The electrochemical response of TET was analysed on the D:CNW electrode by examining its concentration, as shown in Fig. 4. TET reduces electrochemically generating three distinct peaks at potentials of about −0.16 V ("i" peak), −0.33 V ("ii" peak), and −0.48 V ("iii" peak) *vs* Ag/AgCl/3M KCl. An additional, fourth, weakly separated reduction peak is observed at a potential of −0.58 V ("iv" peak).

Given the similar chemical structure of TET to TNT (see Fig. 5a), a similar electroreduction mechanism is also expected. TET contains an additional fourth nitro moiety in its structure, which differs from 2,4,6-trinitrotoluene, which contains only three $–NO_2$ groups. Negative polarisation of the working electrode, that is immersed in TNT solution, should cause a reduction of three nitro groups to three amine groups [25]. As a result, three cathodic signals are expected. Given that tetryl has an additional nitro group compared to TNT (see Fig. 5a), the presence of another fourth peak originating from the additional nitro group can be expected. Due to the limited literature available on TET electroreduction, a new mechanism for TET reduction has been proposed (Fig. 6), based on existing mechanisms for TNT reduction [25,86].

When comparing the electrochemical response of TET and TNT at the same electrode and pH of 5.70 (Fig. 5b), the initial cathodic peak for TET occurs at −0.10 V, whereas for TNT it appears at −0.31 V. Thus, the reduction of one of the nitro groups requires a lower overpotential compared to 2,4,6-trinitrotoluene. It should be noted that TET has an additional nitro group attached to the nitrogen (in the case of TNT $–NO_2$ always links to the carbon atom). According to a mass spectrometric analysis of TET [87], this group will fragment first. So it is expected, that the "i" peak originates from the electroreduction of the only group of TET that is attached to nitrogen (see the first stage of reaction in Fig. 6). Next, based on density functional theory (DFT) calculations made by Chua *et al.* [86], the nitro group in the ortho position (with respect to the methyl group) will next undergo a further reduction (second stage). The DFT results agree with the experiment carried out for 2-nitrotoluene and 4-nitrotoluene, in which the reduction overpotential was lower for the $–NO_2$ group substituted in the ortho position [88]. The second group in the ortho position will probably be the next group to be reduced, followed by the para group [86].

The complete reduction of TNT to 2,4,6-triaminotoluene is believed to require 18 electrons and 18 protons [25,86]. In the case of TET, an additional 6 electrons and 6 protons are needed for the irreversible reduction of the fourth $–NO_2$ group, resulting in a total of 24 electrons and 24 protons. This process can be viewed as a proton-electron coupled reaction, where protons and electrons are exchanged in a single kinetic step [89].

The effect of the presence of protons on the TET reduction reaction becomes especially visible when comparing the results obtained in 0.1 M

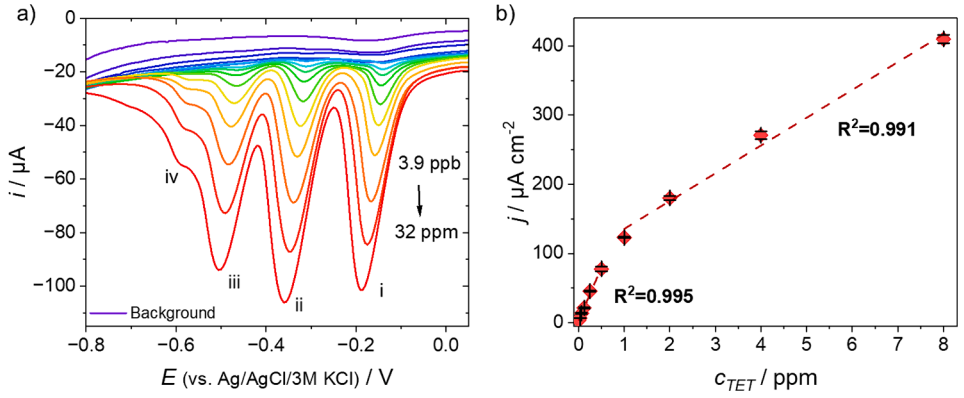

Fig. 4. a) DPV of TET measured on D:CNW in 0.1 M PBS, pH = 6.75; b) concentration dependence of TET on D:CNW based on the magnitude of "i" reduction peak (with the error bars indicating the standard deviation).

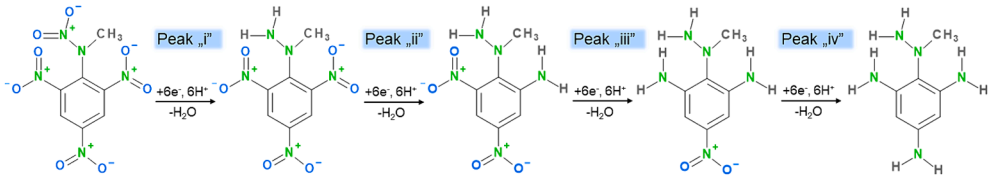

Fig. 6. Proposed mechanism of TET electroreduction.

PBS with different pH (see Fig. S6, SI 9). Depending on the solution pH, the position of the cathodic peak maximum shifts. As the pH increases, peak "i" peak position changes from *ca.* −0.11 V at pH = 5.70, to *ca.* −0.15 V for pH = 6.75 and reaches the peak at −0.19 V (*vs* Ag/AgCl/3M KCl) for pH of 8.00. Similar behaviour was observed during our previous studies concerning TNT [25]. pH dependence of the cathodic "i" peak potential is linear with a slope of 37.1 mV / pH (see Fig. S7, SI 9). The shift in the peak being pH dependent further increases confidence that the mechanism proposed (which is proton dependent) is valid because as the H^+ concentration increases the potential required to perform the first reduction is lower (closer to 0).

Based on the most characteristic TET peak, *i.e.* peak "i", a calibration curve was plotted against TET concentration (Fig. 4b). Two regions of linear relation between the peak current and concentration of TET were observed: 3.9 – 500 ppb and 1 – 8 ppm (see Table 3).

Based on the calibration curve obtained for the low concentrations, a high value of sensitivity for the detection of TET on the D:CNW electrode of 153.0 μA cm^{-2} ppm^{-1} was obtained. Next, by using Eq. 2, LOD calculations were performed. The D:CNW shows very low LOD value of 17 ppb (59.2 nM). The high sensitivity of the electrode is likely due to the high amount of sp^2 carbon building up the dendrite-like structures. The sp^2 carbon has been shown to play a key role in the detection of nitroaromatic compounds, through π-donor–acceptor interactions between the electrode and TET [24,90]. The outstanding sensitivity of the D:CNW electrode in detecting nitroaromatic compounds is demonstrated by comparing the current heights observed in a PBS solution with 2 ppm 2,4-DNT on several carbon electrodes: GC, $BDD_{as\ grown}$, $BDD_{acid\ cleaned}$ (Fig. S8, SI 10). The intensity of the "i" peak is significantly greater for the D:CNW electrode, exceeding 16-fold.

D:CNW exhibited good repeatability. Based on the maximal "i" peak current measured with five different electrodes to detect 1 ppm TET in 0.1 M PBS (pH = 6.75) solution, the calculated relative standard deviation (RSD) value was 2.64 %, whereas the mean recovery was 90.40%.

Two approaches were used to examine the stability of the D:CNW sample by comparing: *i)* the surface morphology of the D:CNW before and after 3,000 cycles in the range 0 to −0.95 V (*vs* Ag/AgCl/3 M KCl) in 0.1 M PBS using CV (ν = 100 mV s^{-1}), which could show the effect of long term polarisation on the sample (Fig. 5c); *ii)* by comparing the impedance spectra collected during a 14-day period of storing the sample in DI water (Fig. 5d). The first test showed no noticeable differences in the D:CNW structure – dendritic structures have not been degraded, their shape is preserved despite long cycling of the sample. The second test was evaluated by measuring the EIS spectra of 4 carbon electrodes. EIS was performed in 1 mM RuHex redox mediator in 1 M KCl at formal potential over a period of 2 weeks. After each measurement, the samples were washed with demineralised water and afterwards stored in DI water between the electrochemical tests. Comparing the results of the Nyquist plot shown in Fig. 5d, no significant changes in the impedimetric spectrum could be seen over time. The obtained spectra were fitted with the same EEC used for the electrochemical characterization of the D:CNW electrode in order to improve the comparability of the results. After 14. days no significant differences in the charge transfer resistance were observed (R_{ct} slightly increased from 0.5 ± 0.2 Ω cm^2 to 0.7 ± 0.6 Ω cm^2).

A variety of nitroaromatic chemicals, including TET, TNT, 2,4-DNT, 2,6-DNT, and nitrotoluenes, can be detected by D:CNW electrodes; they are not just selective for TET (see Fig. 5b). For environmental monitoring, our primary concern is to detect potentially harmful chemicals rapidly and in a cost-effective manner. In turn, the control of production processes should also cover a wider range of compounds, as explosives factories rarely focus on a single compound. In this instance, the sensor's ability to detect a wide range of explosive compounds and their derivatives is undoubtedly advantageous. It's important to emphasize that the electrochemical reaction of TET is highly distinctive: electroreduction generates four cathodic peaks, and therefore it should be easy to detect. Moreover, the "i" peak appears relatively fast (at a small overpotential), which also distinguishes it from other nitroaromatic compounds.

The final step was assessing the feasibility of utilising the electrochemical sensor in practical settings, including samples obtained from industrial and post-industrial locations as outlined in sections 2.5 and SI 4. Despite the challenging environmental conditions and non-uniformly flat background current response, the presence of TET was successfully detected in all TET spiked samples (Fig. 7).

Fresh water sample collected from the site of the "Zachem Chemical Plant" in Bydgoszcz contains a greater amount of organic matter compared to the samples from the Gdańsk landfill area (chemical oxygen demand (COD) = 59.2 mg L^{-1} obtained for ZCP and COD below 10 mg L^{-1} for samples MWMP-P and MWMP-W). Moreover, it is estimated that 93.9% of total nitrogen in ZCP is organic nitrogen. The abundant presence of organic matter is expected to diminish the sensitivity of TET detection. The electroreduction process of nitroaromatic compounds leads to the formation of different types of radicals, which are intermediate products [86,91]. These radicals can over-react with this matter, resulting in the reduced sensitivity recorded for the ZCP sample, for which the first well-created peaks are only visible at a TET concentration of 1 ppm (although the background current is relatively flat, Fig. 7a). Therefore, this sample displays only one linear range, which extends from a concentration of 1 ppm to 16 ppm (R^2 = 0.997).

In contrast, samples from the waste site contained extra electroactive compounds, leading to additional peaks visible in background measurements giving a peak at −0.24 V (*vs* Ag/AgCl/3M KCl) and a slight one at −0.0125 V (see Fig. 7b-c). Additional peaks could be seen also at low TET concentration measurements. For 0.125 ppm additional signal is visible at −0.050 V (for the MWMP-P sample), whereas for 0.5 ppm the signal shifted to −0.106 V. The phenomenon is probably related to the reduction of recombinant products: the reduction products generated in the detection of 0.25 ppm of TET adsorbed at the electrode and then with the second scan were reduced at different potentials.

However, it should be emphasised that, despite the presence of electroactive compounds, it was possible to detect 0.125 ppm and 0.25 ppm of TET in MWMP-P and MWMP-W, respectively. Detection capabilities of D:CNW in environmental samples are greater in laboratory samples with high purity and known composition than recorded in

Table 3
Sensing performance of D:CNW electrode towards TET in 0.1 M PBS (pH = 6.75).

Electrode	Linear range	Calibration curves
D:CNW	3.9 – 500 ppb (0.14 – 1.74 μM) 1 – 8 ppm (3.48 – 13.93 μM)	j [μA cm^{-2}] = 153.0 (±5.0) c_{TET} [ppm] + 3.3 (±1.1) j [μA cm^{-2}] = 40.2 (±2.8) c_{TET} [ppm] + 95.4 (±12.8)

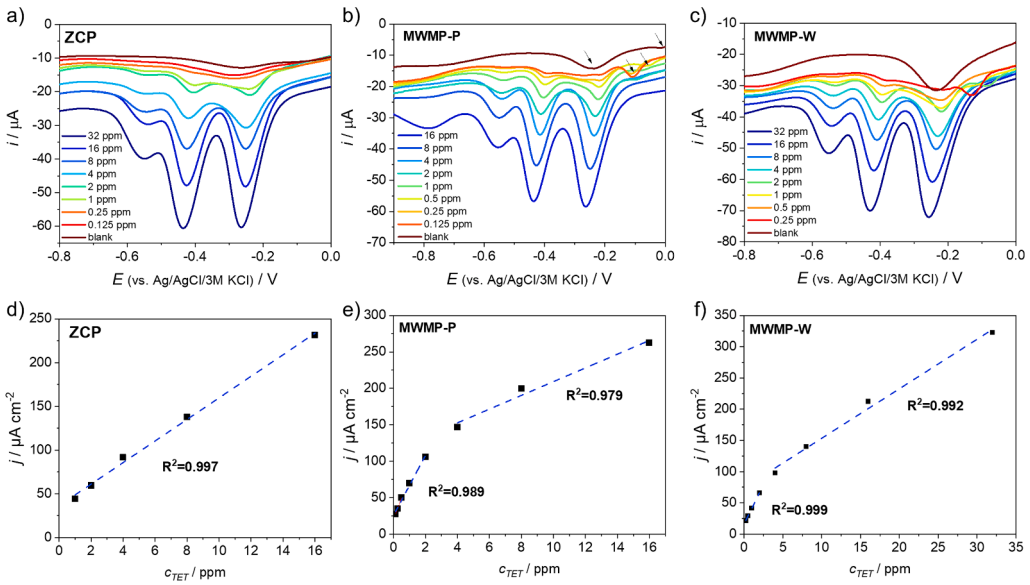

Fig. 7. Detection of TET in a) ZCP, b) MWMP-P, c) MWMP-W samples recorded on D:CNW. Calibration curves prepared from peak "i" for the solution d) ZCP, e) MWMP-P, f) MWMP-W.

environmental samples. It should be noted, however, that the D:CNW electrode response has been tested in very complex matrices originating from industrial and post-industrial sites.

The literature on the electrochemical detection of TET in aqueous samples, and thus having applications in environmental monitoring, is limited. Table 4 summarises the work available in the literature on TET detection (not including chromatographic methods). The work of Bozic *et al.* [92] shows the possibility of using an electrochemical method in the form of square wave voltammetry, however, the study did not cover either linearity or stability ranges, which is a significant drawback. In contrast, the work of Hay *et al.* [93] considers the electroreduction mechanism of TET; however, the solvent is ionic liquids, which do not reflect environmental conditions. It should be noted that D:CNW electrode shows very high sensitivity (LOD = 0.0592 µM) and does not change significantly with time. Moreover, compared to the other electrodes shown in Table 4, the preparation of the D:CNW electrode represents a single step in the form of the MPECVD process. The electrode also does not undergo any post-treatment process.

Table 4
Non-chromatographic methods for the detection of TET in aqueous environment.

Electrode material	Method	Linear range / µM	LOD / µM	Ref.
Modified silica NPs	Optical: fluorescence	ND	0.592	[94]
NA	Optical: fluorescence	3.48 – 17.41	3.483	[95]
Au with MCU[1]	Electrochemical: SWV	ND	0.052	[92]
pTTP-GC[2]	Electrochemical: DPV	0.031 – 0.871	0.031	[33]
GC/P(o-PDA-co-ANI)-Au^{3}_{nano}	Electrochemical: CV	17.41 – 348.26	13.23	[96]
D:CNW	**Electrochemical: DPV**	**0.14 – 1.74 3.48 – 27.90**	**0.0592**	**This work**

ND – no data; NA – not applicable. [1]MCU –11-mercapto-1-undecanol; [2]pTTP-GC – Poly[*meso*-tetrakis(2-thienyl) porphyrin] modified glassy carbon electrode; [3] GC/P(o-PDA-co-ANI)-Au_{nano} – glassy carbon (GC) electrode coated with poly(o-pheny-lenediamine–aniline) film.

4. Conclusions

The study yielded a sp^2-rich carbon nanowall electrode material characterized by a developed surface area in its novel dendrite-like structure. The presence of *ca.* 74–78% sp^2 carbon, a key element for the efficient electrochemical detection of nitroaromatic compounds, was confirmed both by calculating the *D*-parameter within the XPS tests and using the two-window EELS method.

The study successfully developed an electrochemical TET sensor that can be used in both laboratory and environmental samples. Furthermore, the work proposes a mechanism for the electroreduction of TET in aqueous environments. It has been shown that the D:CNW electrode exhibits an exceptional sensitivity of 153.0 µA cm^{-2} ppm^{-1} and an impressive detection limit of 17 ppb. Furthermore, despite a very complex matrix of environmental samples from industrial and post-industrial sites, it was possible to detect 0.125 ppm and 0.25 ppm (depending on the environmental sample) using this electrode.

Different polynitroaromatic compounds have been shown to have different reduction potentials (assuming a constant solution pH). Using the D:CNW electrode, the signal from TET, TNT or DNT can be easily recognised. It was shown that the D:CNW electrode has both cyclic polarisation resistance in PBS solution in the potential range at which nitroaromatic compounds are expected to be present, and does not change significantly over time when the sample is stored in an aqueous environment.

Thus, by leveraging the unique properties of D:CNW, we envision the development of advanced electrochemical sensors capable of rapid, cost-effective and on-site detection of hazardous nitroexplosive compounds, thereby addressing critical needs in environmental monitoring and industrial processes.

CRediT authorship contribution statement

Anna Dettlaff: Writing – review & editing, Writing – original draft, Visualization, Project administration, Methodology, Investigation, Funding acquisition, Formal analysis, Conceptualization. **Małgorzata Szopińska:** Writing – original draft, Resources, Investigation. **Daniel Houghton:** Writing – original draft, Investigation. **Piotr Prasuła:** Resources. **Yisong Han:** Investigation. **Marc Walker:** Investigation, Formal analysis. **Geoff West:** Investigation. **Agata Kamieńska-Duda:** Resources. **Sylwia Fudala-Książek:** Resources. **Michał Sobaszek:**

Writing – original draft, Investigation.

Declaration of competing interest

The authors declare the following financial interests/personal relationships which may be considered as potential competing interests: Anna Dettlaff reports financial support was provided by EEA Grants. If there are other authors, they declare that they have no known competing financial interests or personal relationships that could have appeared to influence the work reported in this paper.

Data availability

The raw research data are visible here: https://doi.org/10.34808/5382-xk57

Acknowledgements

The research leading to these results has received funding from the Norway Grants 2014 - 2021 through the National Centre for Research and Development, Poland [NOR/SGS/NITROsens/0011/2020-00]. The authors thank Prof. Miroslaw Sawczak for performing the Raman measurements. We also acknowledge George Pryer-Freeman for Ti sputtering, Monika Szkudlarek for TET crystallisation and Paweł Rutecki for help with electrochemical measurements. D.H. thanks Johnson Matthey and the Warwick Centre for Diamond Science and Technology for funding. The DS funds of the Faculty of Electronics, Telecommunications, and Informatics of the Gdansk University of Technology are also acknowledged.

Appendix A. Supplementary data

Supplementary data to this article can be found online at https://doi.org/10.1016/j.cej.2024.152620.

References

[1] J.P. Agrawal, High energy materials. Propellants, explosives and pyrotechnics, Wiley-VCH Verlag GmbH, Weinheim, 2010.
[2] A. Amrullah, O. Farobie, R. Widyanto, J. Armiyanti, L. Ersis, W. Abbas, M. Jumriani, E. Bella, E. Potensi, E. Caulerpa, S. Pi, A. Dengan, C. Limbah, K. Air, J.E. Hapsari, C. Amri, A. Suyanto, J.R. Hidayati, U. Diponegoro, A. Ridlo, M. Hilir, K. Sumbawa, A. Husni, D.R. Putra, X. Jiping, L. Ruina, D. Haixia, P. Kaewsarn, Q. Yu, F. Kedokteran, U.H. Tuah, R.M. Kosanke, P. Logam, B. Kadmium, M. Nurilmala, E. Anwar, N. Luthfiyana, E. Rosita, W.R. Melani, A. Zulfikar, Suparyanto dan Rosad (2015, I. Tahu, K. Air, N.A. Umar, S. Budi, T.P. Utami, H. Cakrawati, M. Irramah, A. Wicaksana, R. Yunus, N.S. Prihatini, Defence Safty Authority, Defence Ordnance, Munitions and Explosives (OME) Safety Regulator (DOSR), 2020, Chapter 17: Explosive Facilities - Safety Precautions, in: JSP 482 Minist. Def. Explos. Regul., 2013. https://www.gov.uk/government/publications/dsa03-ome-part-2-in-service-and-operational-safety-management-of-ome (available 28.05.24).
[3] Agency for Toxic Substances and Registry, Public Health Statement Tetryl, 1995, Agency Toxic Subst. Regist. (2015) 5–8. https://www.atsdr.cdc.gov/ToxProfiles/tp80-c1-b.pdf (available 28.05.24).
[4] W. Wen-Zong, N.D. Speciner, G.S. Edwards, Mutagenic activity of tetryl, a nitroaromatic explosive, in three microbial test systems, Toxicol. Lett. 5 (1980) 11–17, https://doi.org/10.1016/0378-4274(80)90142-3.
[5] V.H. Adams, Wildlife Toxicity Assessment for N-Methyl-N-2,4,6-Tetranitroaniline (Tetryl), Elsevier Inc., 2015. doi: 10.1016/b978-0-12-800020-5.00010-7.
[6] G.B. Fitzgerald, A. Austin, N. Diguilio, Acute toxicity evaluation of nitroaromatic compounds, 1991. https://apps.dtic.mil/sti/citations/ADA236352 (available 28.05.24).
[7] M. Nipper, R.S. Carr, J.M. Biedenbach, R.L. Hooten, K. Miller, S. Saepoff, Development of marine toxicity data for ordnance compounds, Arch. Environ. Contam. Toxicol. 41 (2001) 308–318, https://doi.org/10.1007/s002440010253.
[8] O. Drzyzga, T. Gorontzy, A. Schmidt, K.H. Blotevogel, Toxicity of explosives and related compounds to the luminescent bacterium Vibrio fischeri NRRL-B-11177, Arch. Environ. Contam. Toxicol. 28 (1995) 229–235, https://doi.org/10.1007/BF00217621.
[9] P. Kovacic, R. Somanathan, Nitroaromatic compounds: Environmental toxicity, carcinogenicity, mutagenicity, therapy and mechanism, J. Appl. Toxicol. 34 (2014) 810–824, https://doi.org/10.1002/jat.2980.
[10] G. Zhou, H. Pu, J. Chang, X. Sui, S. Mao, J. Chen, Real-time electronic sensor based on black phosphorus/Au NPs/DTT hybrid structure: Application in arsenic detection, Sensors Actuators, B Chem. 257 (2018) 214–219, https://doi.org/10.1016/j.snb.2017.10.132.
[11] W.A. Alfaraj, B. McMillan, A.M. Ducatman, C.L. Werntz, Tetryl exposure: Forgotten hazards of antique munitions, Ann. Occup. Environ. Med. 28 (2016) 16–18, https://doi.org/10.1186/s40557-016-0102-7.
[12] D.N. Khue, T.D. Lam, N. Van Chat, V.Q. Bach, D.B. Minh, V.D. Loi, N. Van Anh, Simultaneous degradation of 2,4,6-trinitrophenyl-N-methylnitramine (Tetryl) and hexahydro-1,3,5-trinitro-1,3,5 triazine (RDX) in polluted wastewater using some advanced oxidation processes, J. Ind. Eng. Chem. 20 (2014) 1468–1475, https://doi.org/10.1016/j.jiec.2013.07.033.
[13] U.S. Department of Health and Human Services, Toxicological Profile for Tetryl (2,4,6-Trinitrophenyl-N-methylnitramine), 1995, https://www.atsdr.cdc.gov/ToxProfiles/tp80.pdf (available 28.05.2024).
[14] S.S. Talmage, D.M. Opresko, C.J. Maxwell, C.J.E. Welsh, M. Cretella, P.H. Reno, B. Daniel, Reviews of Environmental Contamination and Toxicology, Springer, 1999.
[15] T.B. Stanford, Jr, The determination of tetryl and 2,3-, 2,4-, 2,5-, 2,6-, 3,4- and 3,5-dinitrotoluene using high performance liquid chromatography, 1977. https://apps.dtic.mil/sti/citations/ADA042598 (available 28.05.24).
[16] M.E. Fuller, J. Kruczek, R.L. Schuster, P.L. Sheehan, P.M. Arienti, Bioslurry treatment for soils contaminated with very high concentrations of 2,4,6-trinitrophenylmethylnitramine (tetryl), J. Hazard. Mater. 100 (2003) 245–257, https://doi.org/10.1016/S0304-3894(03)00115-8.
[17] S.D. Harvey, R.J. Fellows, J.A. Campbell, D.A. Cataldo, Determination of the explosive 2,4,6-trinitrophenylmethylnitramine (tetryl) and its transformation products in soil, J. Chromatogr. a. 605 (1992) 227–240, https://doi.org/10.1016/0021-9673(92)85241-K.
[18] Q. He, B. Wang, J. Liang, J. Liu, B. Liang, G. Li, Y. Long, G. Zhang, H. Liu, Research on the construction of portable electrochemical sensors for environmental compounds quality monitoring, Mater. Today Adv. 17 (2023) 100340, https://doi.org/10.1016/j.mtadv.2022.100340.
[19] A.C. Power, B. Gorey, S. Chandra, J. Chapman, Carbon nanomaterials and their application to electrochemical sensors: A review, Nanotechnol. Rev. 7 (2018) 19–41, https://doi.org/10.1515/ntrev-2017-0160.
[20] A. Qureshi, W.P. Kang, J.L. Davidson, Y. Gurbuz, Review on carbon-derived, solid-state, micro and nano sensors for electrochemical sensing applications, Diam. Relat. Mater. 18 (2009) 1401–1420, https://doi.org/10.1016/j.diamond.2009.09.008.
[21] L.S. Porto, D.N. Silva, A.E.F. de Oliveira, A.C. Pereira, K.B. Borges, Carbon nanomaterials: Synthesis and applications to development of electrochemical sensors in determination of drugs and compounds of clinical interest, Rev. Anal. Chem. 38 (2020) 1–16, https://doi.org/10.1515/revac-2019-0017.
[22] A. Dettlaff, M. Sobaszek, T. Klimczuk, R. Bogdanowicz, Enhanced electrochemical kinetics of highly-oriented (111)-textured boron-doped diamond electrodes induced by deuterium plasma chemistry, Carbon 174 (2021) 594–604, https://doi.org/10.1016/j.carbon.2020.11.096.
[23] R. Ramachandran, T.-W. Chen, S.-M. Chen, T. Baskar, R. Kannan, P. Elumalai, P. Raja, T. Jeyapragasam, K. Dinakaran, G. Peter Gnana Kumar, A review of the advanced developments of electrochemical sensors for the detection of toxic and bioactive molecules, Inorg. Chem. Front. 6 (2019) 3418–3439, https://doi.org/10.1039/c9qi00602h.
[24] M. Riskin, R. Tel-vered, T. Bourenko, E. Granot, I. Willner, Imprinting of molecular recognition sites through electropolymerization of functionalized Au nanoparticles: development of an electrochemical TNT sensor based on π -donor - acceptor interactions, J. Am. Chem. Soc. 130 (2008) 9726–9733, https://doi.org/10.1021/ja711278c.
[25] A. Dettlaff, P. Jakóbczyk, M. Ficek, B. Wilk, M. Szala, J. Wojtas, T. Ossowski, R. Bogdanowicz, Electrochemical determination of nitroaromatic explosives at boron-doped diamond/graphene nanowall electrodes: 2,4,6-trinitrotoluene and 2,4,6-trinitroanisole in liquid effluents, J. Hazard. Mater. 387 (2020) 121672, https://doi.org/10.1016/j.jhazmat.2019.121672.
[26] A.M. O'Mahony, J. Wang, Nanomaterial-based electrochemical detection of explosives: A review of recent developments, Anal. Methods. 5 (2013) 4296–4309, https://doi.org/10.1039/c3ay40636a.
[27] H.X. Zhang, J.H. Zhang, Voltammetric detection of nitroaromatic compounds using carbon-nanomaterials-based electrodes, Can. J. Chem. 89 (2011) 8–12, https://doi.org/10.1139/V10-064.
[28] S.M. Tan, C.K. Chua, M. Pumera, Graphenes prepared from multi-walled carbon nanotubes and stacked graphene nanofibers for detection of 2,4,6-trinitrotoluene (TNT) in seawater, Analyst 138 (2013) 1700–1704, https://doi.org/10.1039/c3an00089c.
[29] J. Wang, S.B. Hocevar, B. Ogorevc, Carbon nanotube-modified glassy carbon electrode for adsorptive stripping voltammetric detection of ultratrace levels of 2,4,6-trinitrotoluene, Electrochem. Commun. 6 (2004) 176–179, https://doi.org/10.1016/j.elecom.2003.11.010.
[30] A. Dettlaff, P. Jakóbczyk, M. Sobaszek, M. Ficek, B. Dec, A. Łuczkiewicz, M. Szala, J. Wojtas, T. Ossowski, R. Bogdanowicz, Electrochemical detection of 4,4',5,5'-Tetranitro-1H,1'H-2,2'-biimidazole on boron-doped diamond/graphene nanowall electrodes, IEEE Sens. J. 20 (2020) 9637–9643, https://doi.org/10.1109/JSEN.2020.2973451.
[31] W. Białobrzeska, M. Ficek, B. Dec, S. Osella, B. Trzaskowski, A. Jaramillo-Botero, M. Pierpaoli, M. Rycewicz, Y. Dashkevich, T. Łęga, N. Malinowska, Z. Cebula, D. Bigus, D. Firganek, E. Bięga, K. Dziąbowska, M. Brodowski, M. Kowalski, M. Panasiuk, B. Gromadzka, S. Żołędowska, D. Nidzworski, K. Pyrć, W.A. Goddard, R. Bogdanowicz, Performance of electrochemical immunoassays for clinical diagnostics of SARS-CoV-2 based on selective nucleocapsid N protein detection:

Boron-doped diamond, gold and glassy carbon evaluation, Biosens. Bioelectron. 209 (2022), https://doi.org/10.1016/j.bios.2022.114222.
[32] R.C. Thomson, S. Newman, G.D. West, M. Karunaratne, Microstructural evolution in coated superalloy systems, Energy Mater Mater. Sci. Eng. Energy Syst. 4 (2009) 11–16, https://doi.org/10.1179/174892310X12645184130523.
[33] W. Chen, Y. Wang, C. Brückner, C. Ming, Y. Lei, Sensors and Actuators B : Chemical Poly [meso -tetrakis (2-thienyl) porphyrin] for the sensitive electrochemical detection of explosives, Sensors Actuators B Chem. 147 (2010) 191–197, https://doi.org/10.1016/j.snb.2010.03.046.
[34] Y.T. Yew, A. Ambrosi, M. Pumera, Nitroaromatic explosives detection using electrochemically exfoliated graphene, Sci. Rep. 6 (2016) 1–11, https://doi.org/10.1038/srep33276.
[35] Ş. Sağlam, A. Üzer, E. Erçağ, R. Apak, Electrochemical Determination of TNT, DNT, RDX, and HMX with Gold Nanoparticles/Poly(Carbazole-Aniline) Film-Modified Glassy Carbon Sensor Electrodes Imprinted for Molecular Recognition of Nitroaromatics and Nitramines, Anal. Chem. 90 (2018) 7364–7370, https://doi.org/10.1021/acs.analchem.8b00715.
[36] R.A. Soomro, O.P. Akyuz, H. Akin, R. Ozturk, Z.H. Ibupoto, Highly sensitive shape dependent electro-catalysis of TNT molecules using Pd and Pd-Pt alloy based nanostructures, RSC Adv. 6 (2016) 44955–44962, https://doi.org/10.1039/c6ra05588e.
[37] A. Dettlaff, M. Rycewicz, M. Ficek, A. Wieloszyńska, M. Szala, J. Ryl, R. Bogdanowicz, Conductive printable electrodes tuned by boron-doped nanodiamond foil additives for nitroexplosive detection, Microchim. Acta. 189 (2022) 1–11, https://doi.org/10.1007/s00604-022-05371-w.
[38] S. Kurita, A. Yoshimura, H. Kawamoto, T. Uchida, K. Kojima, M. Tachibana, P. Molina-Morales, H. Nakai, Raman spectra of carbon nanowalls grown by plasma-enhanced chemical vapor deposition, J. Appl. Phys. 97 (2005), https://doi.org/10.1063/1.1900297.
[39] M. Hiramatsu, K. Shiji, H. Amano, M. Hori, Fabrication of vertically aligned carbon nanowalls using capacitively coupled plasma-enhanced chemical vapor deposition assisted by hydrogen radical injection, Appl. Phys. Lett. 84 (2004) 4708–4710, https://doi.org/10.1063/1.1762702.
[40] K. Shiji, M. Hiramatsu, A. Enomoto, M. Nakamura, H. Amano, M. Hori, Vertical growth of carbon nanowalls using rf plasma-enhanced chemical vapor deposition, Diam. Relat. Mater. 14 (2005) 831–834, https://doi.org/10.1016/j.diamond.2004.10.021.
[41] Y. Wu, P. Qiao, T. Chong, Z. Shen, Carbon nanowalls grown by microwave plasma enhanced chemical vapor deposition, Adv. Mater. 14 (2002) 64–67, https://doi.org/10.1002/1521-4095(20020104)14:1<64::AID-ADMA64>3.0.CO;2-G.
[42] Y. Wu, B. Yang, B. Zong, H. Sun, Z. Shen, Y. Feng, Carbon nanowalls and related materials, J. Mater. Chem. (2004) 469–477, https://doi.org/10.1039/b311682d.
[43] P. Dyakonov, K. Mironovich, S. Svyakhovskiy, O. Voloshina, S. Dagesyan, A. Panchishin, N. Suetin, V. Bagratashvili, P. Timashev, E. Shirshin, S. Evlashin, Carbon nanowalls as a platform for biological SERS studies, Sci. Rep. 7 (2017) 4–10, https://doi.org/10.1038/s41598-017-13087-8.
[44] A. Olejnik, M. Ficek, M. Szkodo, A. Stanisławska, J. Karczewski, J. Ryl, A. Dołęga, K. Siuzdak, R. Bogdanowicz, Tailoring diffusional fields in zwitterion/dopamine copolymer electropolymerized at carbon nanowalls for sensitive recognition of neurotransmitters, ACS Nano. 16 (2022) 13183–13198, https://doi.org/10.1021/acsnano.2c06406.
[45] P. Russo, M. Xiao, N.Y. Zhou, Carbon nanowalls: A new material for resistive switching memory devices, Carbon 120 (2017) 54–62, https://doi.org/10.1016/j.carbon.2017.05.004.
[46] S.A. Evlashin, Y.M. Maksimov, P.V. Dyakonov, A.A. Pilevsky, K.I. Maslakov, Y. A. Mankelevich, E.N. Voronina, S.V. Vavilov, A.A. Pavlov, E.V. Zenova, I. S. Akhatov, N.V. Suetin, N-doped carbon nanowalls for power sources, Sci. Rep. 9 (2019) 1–7, https://doi.org/10.1038/s41598-019-43001-3.
[47] Z.H. Ni, H.M. Fan, Y.P. Feng, Z.X. Shen, B.J. Yang, Y.H. Wu, Raman spectroscopic investigation of carbon nanowalls, J. Chem. Phys. 124 (2006), https://doi.org/10.1063/1.2200353.
[48] Z. Liu, A.F. Sartori, J.G. Buijnsters, Role of sp2 carbon in non-enzymatic electrochemical sensing of glucose using boron-doped diamond electrodes, Electrochem. Commun. 130 (2021), https://doi.org/10.1016/j.elecom.2021.107096.
[49] M. Zhou, Z. Zhai, L. Liu, C. Zhang, Z. Yuan, Z. Lu, B. Chen, D. Shi, B. Yang, Q. Wei, N. Huang, X. Jiang, Controllable synthesized diamond/CNWs film as a novel nanocarbon electrode with wide potential window and enhanced S/B ratio for electrochemical sensing, Appl. Surf. Sci. 551 (2021) 149418, https://doi.org/10.1016/j.apsusc.2021.149418.
[50] R.C. Engstrom, Electrochemical Pretreatment of Glassy Carbon Electrodes, Anal. Chem. 54 (1982) 2310–2314, https://doi.org/10.1021/ac00250a038.
[51] A. Deshpande, S. Rawat, I.M. Patil, S. Rane, T. Bhaskar, S.B. Ogale, S. Hotha, Converting renewable saccharides to heteroatom doped porous carbons as supercapacitor electrodes, Carbon n. y. 214 (2023) 118368, https://doi.org/10.1016/j.carbon.2023.118368.
[52] T. Oshiro, M. Yamazato, A. Higa, M. Toguchi, Raman analysis of trans-polyacetylene chains in hydrogenated amorphous carbon films, Japanese J. Appl. Physics, Part 1 Regul. Pap. Short Notes Rev. Pap. 46 (2007) 756–760, https://doi.org/10.1143/JJAP.46.756.
[53] A.C. Ferrari, J. Robertson, Origin of the 1150 − cm−1 Raman mode in nanocrystalline diamond, Phys. Rev. B - Condens. Matter Mater. Phys. 63 (2001) 2–5, https://doi.org/10.1103/PhysRevB.63.121405.
[54] O. Frank, M. Mohr, J. Maultzsch, C. Thomsen, I. Riaz, R. Jalil, K.S. Novoselov, G. Tsoukleri, J. Parthenios, K. Papagelis, L. Kavan, C. Galiotis, Raman 2D-band splitting in graphene: Theory and experiment, ACS Nano. 5 (2011) 2231–2239, https://doi.org/10.1021/nn103493g.
[55] L. Bokobza, J.-L. Bruneel, M. Couzi, Raman spectra of carbon-based materials (from graphite to carbon black) and of some silicone composites, C. 1 (2015) 77–94, https://doi.org/10.3390/c1010077.
[56] A. Cuesta, P. Dhamelincourt, J. Laureyns, A. Martínez-Alonso, J.M.D. Tascón, Raman microprobe studies on carbon materials, Carbon 32 (1994) 1523–1532, https://doi.org/10.1016/0008-6223(94)90148-1.
[57] A. Dettlaff, M. Sawczak, E. Klugmann-Radziemska, D. Czylkowski, R. Miotk, M. Wilamowska-Zawłocka, High-performance method of carbon nanotubes modification by microwave plasma for thin composite films preparation, Rsc Adv. 7 (2017) 31940–31949, https://doi.org/10.1039/C7RA04707J.
[58] L. de S. Vieira, A review on the use of glassy carbon in advanced technological applications, Carbon N. Y. 186 (2022) 282–302, https://doi.org/10.1016/j.carbon.2021.10.022.
[59] A.L. Hamon, J. Verbeeck, D. Schryvers, J. Benedikt, R.M.C.M.v.d. Sanden, ELNES study of carbon K-edge spectra of plasma deposited carbon films, J. Mater. Chem. 14 (2004) 2030–2035, https://doi.org/10.1039/b406468m.
[60] K. Okada, K. Kimoto, S. Komatsu, S. Matsumoto, Sp2 bonding distributions in nanocrystalline diamond particles by electron energy loss spectroscopy, J. Appl. Phys. 93 (2003) 3120–3122, https://doi.org/10.1063/1.1544443.
[61] J. Bruley, D.B. Williams, J.J. Cuomo, D.P. Pappas, Quantitative near-edge structure analysis of diamond-like carbon in the electron microscope using a two-window method, J. Microsc. 180 (1995) 22–32, https://doi.org/10.1111/j.1365-2818.1995.tb03653.x.
[62] M. Ficek, B. Dec, K.J. Sankaran, K. Gajewski, P. Tatarczak, I. Wlasny, A. Wysmolek, K. Haenen, T. Gotszalk, R. Bogdanowicz, Stable field electron emission and plasma illumination from boron and nitrogen co-doped edge-rich diamond-enhanced carbon nanowalls, Adv. Mater. Interfaces. 8 (2021) 1–11, https://doi.org/10.1002/admi.202100464.
[63] J. Birrell, J.A. Carlisle, O. Auciello, D.M. Gruen, J.M. Gibson, Morphology and electronic structure in nitrogen-doped ultrananocrystalline diamond, Appl. Phys. Lett. 81 (2002) 2235–2237, https://doi.org/10.1063/1.1503153.
[64] K. Siuzdak, M. Ficek, M. Sobaszek, J. Ryl, M. Gnyba, P. Niedziałkowski, N. Malinowska, J. Karczewski, R. Bogdanowicz, Boron-enhanced growth of micron-scale carbon-based nanowalls: a route toward high rates of electrochemical biosensing, ACS Appl. Mater. Interfaces. 9 (2017) 12982–12992, https://doi.org/10.1021/acsami.6b16860.
[65] W. Zhao, J. Gebhardt, K. Gotterbarm, O. Höfert, C. Gleichweit, C. Papp, A. Görling, H.P. Steinrück, Gold intercalation of boron-doped graphene on Ni(111): XPS and DFT study, J. Phys. Condens. Matter. 25 (2013), https://doi.org/10.1088/0953-8984/25/44/445002.
[66] X. Chen, X. Wang, D. Fang, A review on C1s XPS-spectra for some kinds of carbon materials, Fullerenes Nanotub. Carbon Nanostructures. 28 (2020) 1048–1058, https://doi.org/10.1080/1536383X.2020.1794851.
[67] M. Leng, X. Huang, W. Xiao, J. Ding, B. Liu, Y. Du, J. Xue, Enhanced oxygen evolution reaction by Co-O-C bonds in rationally designed Co3O4/graphene nanocomposites, Nano Energy. 33 (2017) 445–452, https://doi.org/10.1016/j.nanoen.2017.01.061.
[68] D.J. Morgan, Comments on the XPS analysis of carbon materials, C. 7 (2021) 51, https://doi.org/10.3390/c7030051.
[69] M.K. Rabchinskii, S.A. Ryzhkov, D.A. Kirilenko, N.V. Ulin, M.V. Baidakova, V. V. Shnitov, S.I. Pavlov, R.G. Chumakov, D.Y. Stolyarova, N.A. Besedina, A. V. Shvidchenko, D.V. Potorochin, F. Roth, D.A. Smirnov, M.V. Gudkov, M. Brzhezinskaya, O.I. Lebedev, V.P. Melnikov, P.N. Brunkov, From graphene oxide towards aminated graphene: facile synthesis, its structure and electronic properties, Sci. Rep. 10 (2020) 1–12, https://doi.org/10.1038/s41598-020-63935-3.
[70] K. Dave, K.H. Park, M. Dhayal, Two-step process for programmable removal of oxygen functionalities of graphene oxide: functional, structural and electrical characteristics, RSC Adv. 5 (2015) 95657–95665, https://doi.org/10.1039/c5ra18880f.
[71] K.J. Sankaran, M. Ficek, K. Panda, C.J. Yeh, M. Sawczak, J. Ryl, K.C. Leou, J. Y. Park, I.N. Lin, R. Bogdanowicz, K. Haenen, Boron-doped nanocrystalline diamond-carbon nanospike hybrid electron emission source, ACS Appl. Mater. Interfaces. 11 (2019) 48612–48623, https://doi.org/10.1021/acsami.9b17942.
[72] R.M. Chrenko, Boron, the dominant acceptor in semiconducting diamond, Phys. Rev. B 7 (1973) 4560–4567, https://doi.org/10.1103/PhysRevB.7.4560.
[73] N. Yang, S. Yu, J.V. MacPherson, Y. Einaga, H. Zhao, G. Zhao, G.M. Swain, X. Jiang, Conductive diamond: Synthesis, properties, and electrochemical applications, Chem. Soc. Rev. 48 (2019) 157–204, https://doi.org/10.1039/c7cs00757d.
[74] M. Sobaszek, K. Siuzdak, J. Ryl, M. Sawczak, S. Gupta, S.B. Carrizosa, M. Ficek, B. Dec, K. Darowicki, R. Bogdanowicz, Diamond phase (sp3-C) rich boron-doped carbon nanowalls (sp2-C): physicochemical and electrochemical properties, J. Phys. Chem. c. 121 (2017) 20821–20833, https://doi.org/10.1021/acs.jpcc.7b06365.
[75] J.C. Lascovich, R. Giorgi, S. Scaglione, Evaluation of the sp2/sp3 ratio in amorphous carbon structure by XPS and XAES, Appl. Surf. Sci. 47 (1991) 17–21, https://doi.org/10.1016/0169-4332(91)90098-5.
[76] A.Y.S. Eng, A. Ambrosi, C.K. Chua, F. Šaněk, Z. Sofer, M. Pumera, Unusual inherent electrochemistry of graphene oxides prepared using permanganate oxidants, Chem. - A Eur. J. 19 (2013) 12673–12683, https://doi.org/10.1002/chem.201301889.
[77] Z.J. Ayres, S.J. Cobb, M.E. Newton, J.V. Macpherson, Quinone electrochemistry for the comparative assessment of sp2 surface content of boron doped diamond

electrodes, Electrochem. Commun. 72 (2016) 59–63, https://doi.org/10.1016/j.elecom.2016.08.024.
[78] R.G. Compton, C.E. Banks, Understanding Voltammetry, World Scientific, 2018.
[79] A.J. Bard, L.R. Faulkner, Electrochemical Methods. Fundamentals and Appliactions., Second, John Wiley @ Sons, INC., 2001. doi: 10.1016/j.aca.2010.06.020.
[80] C.G. Zoski, Handbook of Electrochemistry, Elsevier, 2007.
[81] A.C. Lazanas, M.I. Prodromidis, Electrochemical Impedance Spectroscopy—A Tutorial, ACS Meas. Sci. Au. 3 (2023) 162–193, https://doi.org/10.1021/acsmeasuresciau.2c00070.
[82] L. Huang, Y. Cao, D. Diao, Nanosized graphene sheets induced high electrochemical activity in pure carbon film, Electrochim. Acta. 262 (2018) 173–181, https://doi.org/10.1016/j.electacta.2018.01.027.
[83] E. Luais, M. Boujtita, A. Gohier, A. Tailleur, S. Casimirius, M.A. Djouadi, A. Granier, P.Y. Tessier, Carbon nanowalls as material for electrochemical transducers, Appl. Phys. Lett. 95 (2009), https://doi.org/10.1063/1.3170033.
[84] J. González, E. Laborda, Á. Molina, Voltammetric kinetic studies of electrode reactions: guidelines for detailed understanding of their fundamentals, J. Chem. Educ. 100 (2023) 697–706, https://doi.org/10.1021/acs.jchemed.2c00944.
[85] K. Siuzdak, M. Ficek, M. Sobaszek, J. Ryl, M. Gnyba, Boron enhanced growth of micron-length carbon based nanowall: A route towards high rates electrochemical biosensing, (2017) 5–8. https://doi.org/10.1021/acsami.6b16860.
[86] C.K. Chua, M. Pumera, L. Rulíšek, Reduction pathways of 2,4,6-trinitrotoluene: An electrochemical and theoretical study, J. Phys. Chem. c. 116 (2012) 4243–4251, https://doi.org/10.1021/jp209631x.
[87] V.C.J. Bhasu, M.M. Chaudhri, J. Housden, Rapid mass spectrometric analysis of fragments of trinitrotoluene, picric acid and tetryl generated by laser irradiation, J. Mater. Sci. 26 (1991) 2199–2207, https://doi.org/10.1007/BF00549189.
[88] P. Rutecki, M. Sobaszek, M. Szopińska, A. Dettlaff, Highly Sensitive Voltammetric Determination of Nitroaromatic 4-Nitrotoluene via Hybrid Branched Carbon Nanowalls for Environmental Monitoring [Manuscript in preparation], (2024).
[89] J.J. Warren, T.A. Tronic, J.M. Mayer, Thermochemistry of proton-coupled electron transfer reagents and its implications, Chem. Rev. 110 (2010) 6961–7001, https://doi.org/10.1021/cr100085k.
[90] A.M.O. Mahony, J. Wang, Analytical methods explosives: a review of recent developments, Anal. Methods. 5 (2013) 4296–4309, https://doi.org/10.1039/c3ay40636a.
[91] A. Üzer, Ş. Sağlam, Y. Tekdemir, B. Ustamehmetoğlu, E. Sezer, E. Erçağ, R. Apak, Determination of nitroaromatic and nitramine type energetic materials in synthetic and real mixtures by cyclic voltammetry, Talanta 115 (2013) 768–778, https://doi.org/10.1016/j.talanta.2013.06.047.
[92] R.G. Bozic, A.C. West, Electrochemical detection of 14 common munitions constituents, J. Appl. Electrochem. 44 (2014) 293–300, https://doi.org/10.1007/s10800-013-0624-4.
[93] C.E. Hay, S.K. Linden, D.S. Silvester, Electrochemical Behaviour of Organic Explosive Compounds in Ionic Liquids: Towards Discriminate Electrochemical Sensing, ChemElectroChem. 9 (2022), https://doi.org/10.1002/celc.202200913.
[94] Y. Salinas, E. Climent, R. Martínez-Máñez, F. Sancenón, M.D. Marcos, J. Soto, A. M. Costero, S. Gil, M. Parra, A. Pérez De Diego, Highly selective and sensitive chromo-fluorogenic detection of the Tetryl explosive using functional silica nanoparticles, Chem. Commun. 47 (2011) 11885–11887, https://doi.org/10.1039/c1cc14877j.
[95] S.R. Wallenborg, C.G. Bailey, S.N. Laboratories, P.O. Box, Separation and Detection of Explosives on a Microchip Using Micellar Electrokinetic Chromatography and Indirect Laser-Induced Fluorescence, Anal. Chem. 72 (2000) 1872–1878, https://doi.org/10.1021/ac991382y.
[96] Ş. Sağlam, A. Üzer, Y. Tekdemir, E. Erçağ, R. Apak, Electrochemical sensor for nitroaromatic type energetic materials using gold nanoparticles/poly(o-phenylenediamine-aniline) film modified glassy carbon electrode, Talanta 139 (2015) 181–188, https://doi.org/10.1016/j.talanta.2015.02.059.